Separation Science and Technology
Publication details, including instructions for authors and subscription information:
http://www.informaworld.com/smpp/title~content=t713708471

Macroreticular Resin Columns. I. Modeling of Bead and Filament Packings

J. Michael Brown[a]; David J. Wilson[a]
[a] DEPARTMENTS OF CHEMISTRY AND ENVIRONMENTAL AND WATER RESOURCES, ENGINEERING VANDERBILT UNIVERSITY NASHVILLE, TENNESSEE

To cite this Article Brown, J. Michael and Wilson, David J.(1980) 'Macroreticular Resin Columns. I. Modeling of Bead and Filament Packings', Separation Science and Technology, 15: 8, 1533 — 1553
To link to this Article: DOI: 10.1080/01496398008055605
URL: http://dx.doi.org/10.1080/01496398008055605

SEPARATION SCIENCE AND TECHNOLOGY, 15(8), pp. 1533–1553, 1980

Macroreticular Resin Columns. I. Modeling of Bead and Filament Packings

J. MICHAEL BROWN and DAVID J. WILSON*

DEPARTMENTS OF CHEMISTRY AND ENVIRONMENTAL AND WATER RESOURCES ENGINEERING
VANDERBILT UNIVERSITY
NASHVILLE, TENNESSEE 37235

Abstract

The diffusion of solutes into spherical beads and cylindrical filaments of macroreticular resin is modeled for the ideal and nonideal cases. These results are then used to develop mathematical models for the operation of continuous flow columns packed with such resins. Effects of design and operating parameters on the breakthrough curves of the columns are calculated.

INTRODUCTION

The use of macroreticular resins for the removal of trace organics from water and their recovery for analysis has become quite extensive. Some work has been done with support-bonded silicones (*1*) or Tenax GC polymer (*2*), but the bulk of the studies has been carried out with Rohm and Haas Amberlite XAD-series resins which are highly porous cross-linked polystyrene (XAD-1, 2, and 4) or acrylic ester (XAD-7 and 8) copolymers. These materials combine high capacity with an ease of regeneration and durability that are lacked by activated carbon.

An early analytical study was carried out by Burnham et al. (*3*); they investigated in detail the extraction of a variety of organics from water with XAD-2. Glaze and his co-workers (*4*) concentrated neutral organics from sewage treatment plant effluent on XAD-2, then eluted with ether for analysis. Junk et al. (*5*) sorbed organics from water for analysis using XAD-2 and XAD-4. Glaze and his collaborators (*6*) proposed Total Organic Halogen as a water quality parameter; chlorinated organics are

*To whom correspondence should be addressed.

adsorbed from water onto XAD-2 or XAD-4, eluted, and analyzed microcoulometrically. Huber and Becker (*7*) presented theory and experimental work on the enrichment of trace organics from liquids by displacement chromatography. Pietrzyk and Chu (*8*) used XAD copolymers in reversed phase gravity flow and high performance liquid chromatography (HPLC). They investigated distribution coefficients for a variety of organics in a number of XAD resins at different pH's, and summarized the wide range of applications of macroreticular resins. Paschal,* Bicknell, and Siebenmann (*9*) used XAD-2 resin to concentrate the herbicide atrazine for analysis by HPLC. Suzuki and his co-workers (*10*) extracted the herbicide CNP (2,4,6-trichlorophenyl-4'-nitrophenylether) from water with an XAD-2 column before analysis. Tateda and Fritz (*11*) used XAD-4 to sorb organic contaminants from water in a microanalytical method.

These resins have also been used for wastewater treatment. Kennedy (*12*) described the use of XAD-4 for the treatment of wastewaters from the manufacture of chlorinated pesticides; leakage from the columns was less than that resulting when activated carbon was used, and the resin was easily regenerated with isopropanol. Spano et al. (*13*) described the treatment of wastewaters from TNT plants with XAD-2 and activated carbon. The XAD-2 was readily regenerated with acetone. Kim et al. (*14*) reviewed the use of these resins, as well as other techniques, for the adsorption of organic compounds from wastewaters. Farrier, Hines, and Wang (*15*) investigated the adsorption equilibria of benzoic acid and phenol on XAD-8, and modeled the phenol adsorption isotherm accurately with a three-parameter equation. Characteristics and applications of these resins are also discussed in literature available from Rohm and Haas (*16*).

SPHERICAL BEAD PACKING—ANALYSIS

The Amberlite polymeric adsorbents marketed by Rohm and Haas are in the form of spheres in the size range 20–60 mesh. We therefore first examine the diffusion of ideal and nonideal solutes into spheres from a large pool of liquid. These results are then used to construct a computationally tractable model for simulating the operation of a continuous flow resin column. The methods used are rather similar to our earlier work on activated carbon columns (*17*, *18*).

Diffusion into a Sphere—Ideal Case

The diffusion equation in spherical coordinates for spherically symmetrical geometry and an ideal solute is

$$\frac{\partial c}{\partial t} = \frac{D}{r^2}\frac{\partial}{\partial r}\left(r^2\frac{\partial c}{\partial r}\right) \tag{1}$$

where c = concentration of solute in the sphere at (r, t)
D = diffusion constant of solute in the sphere
t = time
r = distance from the center of the sphere

We briefly summarize the well-known solution to this problem by separation of variables.

$$c(r, t) = T(t)R(r) \tag{2}$$

$$\frac{\dot{T}}{T} = \frac{D}{r^2R}\frac{d}{dr}\left(r^2\frac{dR}{dr}\right) = -\lambda \tag{3}$$

This yields $T = \exp(-\lambda t)$ and

$$\frac{d}{dr}\left(r^2\frac{dR}{dr}\right) + \frac{\lambda}{D}r^2R = 0 \tag{4}$$

which is changed by the substitution

$$u = rR \tag{5}$$

into

$$\frac{d^2u}{dr^2} + \frac{\lambda}{D}u = 0 \tag{6}$$

from which we see that

$$u = A_\lambda \cos\sqrt{\frac{\lambda}{D}}\,r + B_\lambda \sin\sqrt{\frac{\lambda}{D}}\,r \tag{7}$$

The requirement that R not be singular at $r = 0$ dictates that $A_\lambda = 0$, and the observation that $c(r, t) =$ constant is a solution to Eq. (1) then permits us to write

$$c(r, t) = c_\infty + \sum_\lambda \frac{B_\lambda}{r}\sin\left(\sqrt{\frac{\lambda}{D}}\,r\right)\exp(-\lambda t) \tag{8}$$

We let r_b be the radius of the sphere, and require as a boundary condition that

$$c(r_b, t) = c_\infty \tag{9}$$

This necessitates that

$$\sin\left(\sqrt{\frac{\lambda}{D}}\,r_b\right) = 0$$

so

$$\lambda = \lambda_n = \left(\frac{n\pi}{r_b}\right)^2 D \tag{10}$$

and

$$c(r, t) = c_\infty + \sum_{n=1}^{\infty} \frac{B_n}{r} \sin \frac{n\pi r}{r_b} \exp\left(\frac{-n^2\pi^2 Dt}{r_b^2}\right) \tag{11}$$

If we assume that initially $c(r, 0) = 0$, $r \neq r_b$, then

$$\sum_{n=1}^{\infty} \frac{B_n}{r} \sin \frac{n\pi r}{r_b} = -c_\infty \tag{12}$$

The B_n's are then obtained by multiplying Eq. (12) by $r \sin (mr/r_b)$ and integrating from 0 to r_b to find

$$B_m = (-1)^m \frac{2r_b}{m\pi} c_\infty \tag{13}$$

and

$$c(r, t) = c_\infty + \frac{2r_b}{r} c_\infty \sum_{n=1}^{\infty} \frac{(-1)^m}{n} \sin \frac{n\pi r}{r_b} \exp\left(\frac{-n^2\pi^2 Dt}{r_b^2}\right) \tag{14}$$

The total quantity of solute in the sphere is given by

$$C(t) = 4\pi \int_0^{r_b} r^2 c(r, t)\, dr \tag{15}$$

which on substitution from Eq. (14) and integration yields

$$C(t) = \frac{4\pi r_b^3 c_\infty}{3}\left[1 - \frac{6}{\pi^2} \sum_{n=1} \frac{1}{n^2} \exp\left(\frac{-n^2\pi^2 Dt}{r_b^2}\right)\right] \tag{16}$$

We note that dC/dt is singular at $t = 0$; physically this is due to the infinite concentration gradient associated with our initial conditions. At large times the decay of the system toward equilibrium approaches

$$C(t) \cong \frac{4\pi r_b^3 c_\infty}{3}\left[1 - \frac{6}{\pi^2} \exp\left(\frac{-\pi^2 Dt}{r_b^2}\right)\right] \tag{17}$$

as the term involving the lowest eigenvalue becomes dominant. We make use of results to be derived later to note that the rate of approach to equilibrium of a spherical bead adsorbent is 1.706 times that of a cylindrical filament of the same radius. The radius of a filament must be 0.766 times that of a sphere for the two to have the same time constant, all other factors being equal.

Diffusion into a Sphere—Nonideal Case

We take as our diffusion equation for the spherically symmetric nonideal case

$$\frac{\partial c}{\partial t} = \frac{D}{kT}\frac{1}{r^2}\frac{\partial}{\partial r}\left(r^2 c \frac{\partial \mu}{\partial r}\right) \tag{18}$$

where $\mu(r, t)$ is the chemical potential of the solute (per molecule) at (r, t), and k and T have their usual meaning.

Since the behavior of the solute in the resin is nonideal, Eq. (18) is nonlinear, so we immediately resort to numerical methods. We partition the sphere into N concentric shells of thickness $\Delta r = r_b/N$, and perform a material balance on the nth shell to obtain

$$\begin{aligned}
&\frac{4}{3}\pi(r_n^3 - r_{n-1}^3)\frac{dc_n}{dt} \\
&= 4\pi r_n^2 \frac{D}{kT}\left\{\frac{(\mu_{n+1} - \mu_n)}{\Delta r}[S(\mu_{n+1} - \mu_n)c_{n+1} + S(\mu_{n+1} - \mu_n)c_n]\right\} \\
&\quad + 4\pi r_{n-1}^2 \frac{D}{kT}\left\{\frac{(\mu_{n-1} - \mu_n)}{\Delta r}[S(\mu_{n-1} - \mu_n)c_{n-1} + S(\mu_n - \mu_{n-1})c_n]\right\}
\end{aligned} \tag{19}$$

$$S(x) = 0, x < 0; \qquad S(x) = 1, x \geq 0$$

We note that

$$r_n = n\Delta r, \qquad n = 1, 2, \ldots, N \tag{20}$$

and that

$$r_n^3 - r_{n-1}^3 = \Delta r^3(3n^2 - 3n + 1) \tag{21}$$

so that Eq. (19) rearranges to give

$$\begin{aligned}
\frac{dc_n}{dt} = \frac{3D}{kT(3n^2 - 3n + 1)\Delta r^2}\{&n^2(\mu_{n+1} - \mu_n)[S(\mu_{n+1} - \mu_n)c_{n+1} \\
&+ S(\mu_n - \mu_{n+1})c_n] + (n-1)^2(\mu_{n-1} - \mu_n)[S(\mu_{n-1} - \mu_n)c_{n-1} \\
&+ S(\mu_n - \mu_{n-1})c_n]\}
\end{aligned} \tag{22}$$

In similar fashion the boundary equations for $n = 1$ and $n = N$ are given by

$$\frac{dc_1}{dt} = \frac{3D}{kT\Delta r^2}(\mu_2 - \mu_1)[S(\mu_2 - \mu_1)c_2 + S(\mu_1 - \mu_2)c_1] \tag{23}$$

and

$$\frac{dc_N}{dt} = \frac{3D}{kT(3N^2 - 3N + 1)\Delta r^2}\{N^2(\mu^0 - \mu_N)[S(\mu^0 - \mu_N)c^0 + S(\mu_N - \mu^0)c_N] + (N-1)^2(\mu_{N-1} - \mu_N)[S(\mu_{N-1} - \mu_N)c_{N-1} + S(\mu_N - \mu_{N-1})c_N]\} \quad (24)$$

In Eq. (24), c^0 is the concentration of solute in the sphere which is in equilibrium with the liquid bathing the sphere, and μ^0 is the chemical potential of the solute in the sphere at this concentration. We let c_s be the concentration of solute in the liquid, and calculate c^0 as follows:

$$\mu(\text{solute in solution}) = \mu(\text{solute in resin}) \quad (25)$$

$$\mu_0{}^s + kT\log_e[\gamma(c_s)c_s] = \mu_0{}^R + kT\log_e\frac{c^0}{1 - c^0/c_{\max}} \quad (26)$$

where $\gamma(c_s)$ is the activity coefficient of the solute in solution and $1/(1 - c^0/c_{\max})$ is taken as the activity coefficient of the solute in the resin. Solving Eq. (26) for c^0 yields

$$c^0 = \frac{K\gamma c_s}{1 + K\gamma c_s/c_{\max}} \quad (27)$$

where

$$K = \exp[(\mu_0{}^s - \mu_0{}^R)/kT] \quad (28)$$

The total quantity of solute in a resin bead is then given by

$$C(t) = \frac{4}{3}\pi\sum_{n=1}^{N}(r_n{}^3 - r_{n-1}^3)c_n(t) \quad (29)$$

$$= \frac{4}{3}\pi\Delta r^3\sum_{n=1}^{N}(3n^2 - 3n + 1)c_n(t) \quad (30)$$

and

$$C(\infty) = \frac{4}{3}\pi r_b{}^3c^0 \quad (31)$$

We may estimate time constants for the decay to equilibrium from the slopes of plots of

$$\log_e[1 - C(t)/C(\infty)] \text{ versus } t$$

Spherical Packing in a Continuous Flow Column

In attempting to use the model discussed in the preceding section for simulating the operation of a continuous flow column, we encounter the same difficulty noted in our earlier work on carbon columns (*17*, *18*). The analysis is conceptually quite simple, but requires such large amounts

of computer time that it is not useful for practical design work. In our activated carbon work we employed a lumped parameter approach in which diffusion into a pore was approximated as a one-step process having a single time constant. In the following treatment we improve this by approximating diffusion into a resin sphere as a two-step process; this yields approximations to the first two exponential terms in Eq. (16) if one is examining the ideal case. We proceed as follows. See Fig. 1.

Let M = number of horizontal slabs used to represent the column
V_r = volume of resin per unit volume of column, $\cong 0.74$ for close-packed spheres of a single size
r_c = radius of column
l_c = length of column
$\Delta r = r_b/2$
$\Delta l_c = l_c/M$
N_r = number of resin spheres per unit volume of column, $\cong 3 \times 0.74/4\pi r_b^3$ for close-packed uniform spheres
V_w = volume of liquid per unit volume of column, $= 1 - V_r$
$Q(t)$ = volumetric flow rate through the column
$c_{\text{infl}}(t)$ = influent solute concentration
c_{3n} = concentration of solute in the liquid phase in the nth slab
c_{2n} = concentration of solute in the outer shells of resin beads in the nth slab
c_{1n} = concentration of solute in the inner cores of resin beads in the nth slab
μ_{in} = chemical potential of solute, $i = 1, 2, 3$; $n = 1, 2, \ldots, M$

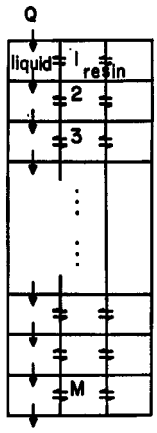

FIG. 1. Lumped parameter model of a macroreticular resin column with diffusion into a resin bead (or filament) modeled as a two-step process.

We partition each resin bead into a spherical core of radius $r_b/2$ and a single surrounding spherical shell; this corresponds to setting $N = 2$ in our previous analysis. We then carry out material balances on the solute in the three regions in each slab: the moving solution, the outer shells of the resin beads, and the inner cores of the resin beads. For the solution phase this yields

$$\Delta l_c \pi r_c^2 V_w \frac{dc_{3n}}{dt} = Q(t)(c_{3n-1} - c_{3n}) - \Delta l_c \pi r_c^2 N_r \frac{4\pi r_b^2 D}{kT} \frac{(\mu_{3n} - \mu_{2n})}{\Delta r} \times [S(\mu_{3n} - \mu_{2n})c_n^0 + S(\mu_{2n} - \mu_{3n})c_{2n}] \quad (32)$$

Here

$$\mu_{3n} = \mu^0 + kT \log_e \frac{c_n^0}{1 - c_n^0/c_{\max}} \quad (33)$$

where

$$c_n^0 = \frac{Kc_{3n}}{1 + Kc_{3n}/c_{\max}} \quad (34)$$

and

$$\mu_{jn} = \mu^0 + kT \log_e \frac{c_{jn}}{1 - c_{jn}/c_{\max}}, \qquad j = 1, 2 \quad (35)$$

Rearrangement of Eq. (32) yields

$$\frac{dc_{3n}}{dt} = \frac{Q(c_{3n-1} - c_{3n})}{\pi r_c^2 \Delta l_c V_w} - \frac{4\pi r_b^2 N_r D}{V_w kT} \frac{(\mu_{3n} - \mu_{2n})}{\Delta r} \times [S(\mu_{3n} - \mu_{2n})c_n^0 + S(\mu_{2n} - \mu_{3n})c_{2n}] \quad (36)$$

The other equations needed are obtained by analogy with Eqs. (23) and (24) (with $N = 2$); they are

$$\frac{dc_{1n}}{dt} = \frac{3D}{kT\Delta r^2}(\mu_{2n} - \mu_{1n})[S(\mu_{2n} - \mu_{1n})c_{2n} + S(\mu_{1n} - \mu_{2n})c_{1n}] \quad (37)$$

and

$$\frac{dc_{2n}}{dt} = \frac{3D}{7kT\Delta r^2}\{4(\mu_{3n} - \mu_{2n})[S(\mu_{3n} - \mu_{2n})c_n^0 + S(\mu_{2n} - \mu_{3n})c_{2n}] + (\mu_{1n} - \mu_{2n})[S(\mu_{1n} - \mu_{2n})c_{1n} + S(\mu_{2n} - \mu_{1n})c_{2n}]\} \quad (38)$$

When $n = 1$ (the column slab which receives the influent), Eq. (36) is modified by replacing c_{3n-1} by $c_{\text{infl}}(t)$. The composition of the column effluent is then given by $c_{3M}(t)$. Equations (36)–(38), $Q(t)$, and $c_{\text{infl}}(t)$ then define the problem. Axial mixing is taken care of by the value of M; the larger this is, the less axial mixing is occurring.

This system of differential equations was integrated by a predictor corrector method (*19*) which we have used previously for simulating activated carbon column (*17, 18*) and clarifier (*20–22*) operation. The algorithm is as follows:

Starter:

$$y^*(\Delta x) = y(0) + \Delta x \frac{dy(0)}{dx} \tag{39}$$

Predictor:

$$y^*[(n + 1)\Delta x] = y[(n - 1)\Delta x] + 2\Delta x \frac{dy}{dx}(n\Delta x) \tag{40}$$

Corrector:

$$y[(n + 1)\Delta x] = y(n\Delta x) + \frac{\Delta x}{2}\left\{\frac{dy}{dx}(n\Delta x) + \frac{dy^*}{dx}[(n + 1)\Delta x]\right\} \tag{41}$$

The algorithm is simple, fast, and stable, provided that Δx (or, in our case, Δt) is not too large.

FILAMENT PACKING—ANALYSIS

One of the problems with bead-type packings is that the spheres must be large enough to permit ready flow of liquid through the column, yet small enough so that the time constant for equilibration between the sphere and the contacting solution is not too long. This time constant increases proportionally to the square of the sphere diameter, as seen above. For resins which can be formed as flexible monofilaments or fibers, this problem could be circumvented by using filaments of quite small diameter as column packing. The long filaments should pack in a fairly open structure, permitting high flow rates with low head loss; the small diameter of the filaments yields short time constants and rapid equilibration, as shown below.

In the following sections we first analyze the diffusion of an ideal solute into a cylindrical filament. We next examine the diffusion of a nonideal solute into a cylindrical filament by numerical methods; we then use these results to construct a mathematical model of the operation of a continuous flow column with filament packing.

Diffusion into a Filament—Ideal Case

Our starting point is the nonideal diffusion equation

$$\frac{\partial c}{\partial t}(r, t) = \frac{D}{kT} \nabla(c \nabla \mu) \tag{42}$$

where $c(r, t)$ = the concentration of solute a distance r from the axis of the filament at time t (see Fig. 2)
$\mu = \mu(r, t)$ = chemical potential (per molecule) of the solute
D = effective diffusion constant of solute in the filament

For the ideal case we have

$$\mu = \mu_0 + kT \log_e c \tag{43}$$

and in cylindrical coordinates Eq. (42) simplifies to

$$\frac{\partial c}{\partial t} = \frac{D}{r} \frac{\partial}{\partial r}\left(r \frac{\partial c}{\partial r}\right) \tag{44}$$

This equation is solved by separation of variables; setting $c(r, t) = R(r)$ $T(t)$ yields in the usual way

$$T = \exp(-\lambda t) \tag{45}$$

$$\frac{1}{r} \frac{d}{dr}\left(r \frac{dR}{dr}\right) + \frac{\lambda}{D} R \tag{46}$$

Equation (46) is Bessel's equation of order zero; we require the solution regular at $r = 0$, so

$$R = J_0\left[\left(\frac{\lambda}{D}\right)^{1/2} r\right] \tag{47}$$

At $r = r_f$, the radius of the filament, the concentration in the resin is always that at equilibrium with the surrounding solution, c_0. $c(r, t) = c_0$ is evidently a solution to Eq. (44), so we may write the general solution to Eq. (44) as

$$c(r, t) = c_0 + \sum_{\lambda} A_\lambda J_0\left[\left(\frac{\lambda}{D}\right)^{1/2} r\right] \exp(-\lambda t) \tag{48}$$

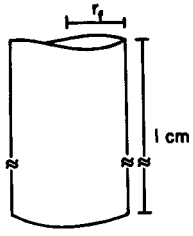

FIG. 2. A segment of a cylindrical resin filament.

When $r = r_f$, $c(r, t) = c_0$, so we must have

$$J_0\left[\left(\frac{\lambda}{D}\right)^{1/2} r_f\right] = 0 \tag{49}$$

which requires that

$$\lambda = \lambda_m = D\left(\frac{x_m}{r_f}\right)^2, \qquad m = 1, 2, \ldots \tag{50}$$

where x_m is the mth root of $J_0(x)$. The unknown coefficients in Eq. (48) are determined by the requirement that, for an initially uncharged resin $[c(r, 0) = 0]$, we must have

$$\sum_{m=1}^{\infty} A_m J_0\left(\frac{x_m r}{r_f}\right) = -c_0 \tag{51}$$

We multiply both sides of Eq. (51) by $rJ_0(x_K r/r_f)$ and integrate from 0 to r_f in the usual way to obtain

$$A_K = \frac{-2c_0}{x_K J_1(x_K)} \tag{52}$$

and

$$c(r, t) = c_0 - 2c_0 \sum_{m=1}^{\infty} \frac{J_0(x_m r/r_f) \exp\left[-D(x_m/r_f)t\right]}{x_m J_1(x_m)} \tag{53}$$

The total quantity of solute adsorbed per unit length of filament at time t we denote by $C(t)$; it is given by

$$C(t) = 2\pi \int_0^{r_f} rc(r, t)\, dr \tag{54}$$

$$= \pi {r_f}^2 c_0 - 4\pi_0 \sum_{m=1}^{\infty} \frac{\exp\left[-D(x_m/r_f)^2 t\right]}{x_m J_1(x_m)} \int_0^{r_f} rJ_0\left(x_m \frac{r}{r_f}\right) dr \tag{55}$$

$$= \pi {r_f}^2 c_0 \left\{1 - 4 \sum_{m=1}^{\infty} \frac{1}{x_m^2} \exp\left[-D(x_m/r_f)^2 t\right]\right\} \tag{56}$$

We estimate the time constant for the approach of the system to equilibrium as the lowest eigenvalue of the system

$$\lambda_1 = D\left(\frac{x_1}{r_f}\right)^2 \tag{57}$$

The first few values of the x_m are 2.405, 5.520, 8.654, 11.79, and 14.93; as m becomes "large" (i.e., >3), $x_m - x_{m-1} \to \pi$, which readily permits the generation of the higher eigenvalues. The eigenvalues are proportional to $1/{r_f}^2$, so the rate of approach to equilibrium increases rapidly with decreasing filament diameter.

Diffusion into a Filament—Nonideal Case

In Fig. 3 we see a cross-section of a filament partitioned into a set of concentric cylindrical shells. We return to the general, nonideal diffusion equation, and write it in cylindrical coordinates,

$$\frac{\partial c}{\partial t} = \frac{D}{kT}\frac{1}{r}\frac{\partial}{\partial r}\left(rc\frac{\partial \mu}{\partial r}\right) \tag{58}$$

We approximate this by examining the fluxes of solute through the inner and outer surfaces of the nth annular shell, which yields

$$\begin{aligned}\pi(r_n^2 - r_{n-1}^2)\frac{dc_n}{dt} &= 2\frac{\pi D}{kT}\left\{\left(\frac{\mu_{n+1} - \mu_n}{\Delta r}\right)[S(\mu_{n+1} - \mu_n)c_{n+1} + S(\mu_n - \mu_{n+1})c_n]r_n \right. \\ &\left. + \left(\frac{\mu_{n-1} - \mu_n}{\Delta r}\right)[S(\mu_{n-1} - \mu_n)c_{n-1} + S(\mu_n - \mu_{n-1})c_n]r_{n-1}\right\} \end{aligned} \tag{59}$$

where $S(x) = 0, \quad x < 0$
$= 1, \quad x \leq 0$
r_n = outer radius of the nth shell, $= n\Delta r$
μ_n = chemical potential of the solute in the nth shell

Substituting $K\Delta r$ for r_K and rearranging Eq. (59) yields

$$\begin{aligned}\frac{dc_n}{dt} = \frac{2D}{(2n-1)\Delta r^2 kT}\{&(\mu_{n+1} - \mu_n)[S(\mu_{n+1} - \mu_n)c_{n+1} + S(\mu_n - \mu_{n+1})c_n]n \\ &+ (\mu_{n-1} - \mu_n)[S(\mu_{n-1} - \mu_n)c_{n-1} + S(\mu_n - \mu_{n-1})c_n](n-1)\}\end{aligned} \tag{60}$$

The boundary conditions are given by

$$\frac{dc_1}{dt} = \frac{2D}{\Delta r^2 kT}\{(\mu_2 - \mu_1)[S(\mu_2 - \mu_1)c_2 + S(\mu_1 - \mu_2)c_1]\} \tag{61}$$

and

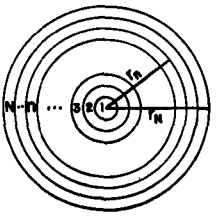

FIG. 3. Partitioning of a resin filament into N annular regions.

$$\frac{dc_N}{dt} = \frac{2D}{(2N-1)\Delta r^2\, dT}\{(\mu^0 - \mu_N)[S(\mu^0 - \mu_N)c^0 + S(\mu_N - \mu^0)c_N]N + (\mu_{N-1} - \mu_N)[S(\mu_{N-1} - \mu_N)c_{N-1} + S(\mu_N - \mu_{N-1})c_N](N-1)\} \tag{62}$$

In Eq. (62) c^0 is the concentration of solute in the resin in equilibrium with a concentration c_s in the solution in contact with the resin. We calculate c^0 from Eq. (27).

The total quantity of solute in a unit length of resin filament is then given by

$$C(t) = \pi \sum_{n=1}^{N} (r_n^2 - r_{n-1}^2)c_n(t) = \pi\Delta r^2 \sum_{n=1}^{N} (2n-1)c_n(t) \tag{63}$$

Also

$$C(\infty) = \pi r_f^2 c^0 \tag{64}$$

and time constants can be estimated from the slopes of plots of $\log_e[C(\infty) - C(t)/C(\infty)]$ versus t. Inspection of Eqs. (60)–(62) shows that the right-hand sides all have a factor $2D/\Delta r^2 kT$. For fixed N we therefore see that as r_N $(= r_f)$ increases, the rate of the system's approach to equilibrium should decrease proportional to r_N^{-2}, as found for the ideal case.

Filament Packing in a Continuous Flow Column

The approach outlined in the last section is not feasible for use in modeling the operation of continuous flow columns because of the excessive amounts of computer time required. We described earlier a closely analogous situation which arose in connection with the modeling of activated carbon columns (*17*, *18*), which we simplified by using a lumped parameter approach that essentially assigns a single time constant to the diffusion of a solute into the pores of a particle of activated carbon. Here we elaborate this approach in such a way as to provide three time constants.

The column is partitioned into a set of horizontal slabs, as was illustrated earlier in Fig. 1. Each filament is then partitioned into three concentric regions; $N = 3$ in Fig. 3.

Let V_r = volume of resin per unit volume of column
r_c = radius of column
l_c = length of column
$\Delta r = r_f/3$
l_r = length of filament per unit volume of column; $l_r = V_r/\pi r_f^2$

V_w = volume of liquid per unit volume of column, $= 1 - V_r$
$Q(t)$ = flow rate through the column
$c^0(t)$ = influent solute concentration

A material balance on the liquid portion of the nth slab yields

$$\Delta l_c \pi r_c^2 V_w \frac{dc_n}{dt} = Q(t)(c_{n-1} - c_n) - \frac{\pi r_c^2 \Delta l_c l_r D}{\Delta r k T} 2\pi r_f(\mu_n - \mu_{3,n}) \times [S(\mu_n - \mu_{3,n})c_n^0 + S(\mu_{3,n} - \mu_n)c_{3,n}] \quad (65)$$

where $c_{m,n}$ = concentration of solute in the mth shell in the resin filaments in the nth slab

$$c_n^0 = \frac{Kc_n}{1 + Kc_n/c_{\max}} \qquad \text{(assume } \gamma = 1 \text{ in Eq. 27)} \quad (66)$$

$$\mu_n = \mu^0 + kT \log_e \frac{c_n^0}{1 - c_n^0/c_{\max}} \quad (67)$$

$$\mu_{3,n} = \mu^0 + kT \log_e \frac{c_{3n}}{1 - c_{3n}/c_{\max}} \quad (68)$$

For the filaments in the nth slab we assume that $N = 3$ and modify the notation in Eqs. (60)–(62) appropriately:

$$\frac{dc_{3n}}{dt} = \frac{2D}{5\Delta r^2 kT} \{(\mu_n - \mu_{3,n})[S(\mu_n - \mu_{3,n})c_n^0 + S(\mu_{3,n} - \mu_n)c_{3,n}] + (\mu_{2,n} - \mu_{3,n})[S(\mu_{2,n} - \mu_{3,n})c_{2,n} + S(\mu_{3,n} - \mu_{2,n})c_{3,n}]2\} \quad (69)$$

$$\frac{dc_{2n}}{dt} = \frac{2D}{3\Delta r^2 kT} \{(\mu_{3,n} - \mu_{2,n})[S(\mu_{3,n} - \mu_{2,n})c_{3,n} + S(\mu_{2,n} - \mu_{3,n})c_{2,n}]2 + (\mu_{1,n} - \mu_{2,n})[S(\mu_{1,n} - \mu_{2,n})c_{1,n} + S(\mu_{2,n} - \mu_{1,n})c_{2,n}]\} \quad (70)$$

$$\frac{dc_{1n}}{dt} = \frac{2D}{\Delta r^2 kT} \{(\mu_{2,n} - \mu_{1,n})[S(\mu_{2,n} - \mu_{1,n})c_{2,n} + S(\mu_{1,n} - \mu_{2,n})c_{1,n}]\} \quad (71)$$

Equation (65) must be modified slightly when $n = 1$ (the top of the column); it becomes

$$\Delta l_c \pi r_c^2 V_w \frac{dc_1}{dt} = Q(t)(c_{\text{infl}} - c_1) - \frac{\pi r_c^2 \Delta l_c l_r D}{\Delta r k T} 2\pi r_r(\mu_1 - \mu_{3,1}) \times [S(\mu_1 - \mu_{3,1})c_1^0 + S(\mu_{3,1} - \mu_1)c_{3,1}] \quad (72)$$

Equations (65)–(72) completely define the problem.

This system of differential equations was integrated by the predictor corrector method described by Eqs. (39)–(41).

RESULTS

We first examined ideal and nonideal diffusion of solute into resin spheres and cylindrical filaments. In both cases the results indicated that a lumped two- or three-compartment model gave results which were in good agreement with the more exact treatments of the process. The details of these results are described elsewhere (*23*).

The effects on the breakthrough curves (plots of effluent solute concentration versus volume of liquid passed through the column) of the diffusion constant for solute penetrating the resin are shown in Figs. 4 (spherical) and 5 (filament). As one would expect, increasing the diffusion constant increases the effluent volume required to produce significant solute breakthrough in both cases.

The effect of bead or filament radius on the breakthrough curves is shown in Figs. 6 and 7, respectively. In either case the larger the radius the smaller the total area of the water–resin interface and the slower the diffusion into the resin, which results in decreasing effluent volumes required to produce breakthrough as radius increases. Increasing the influent flow rate causes column performance to deteriorate, as shown in Figs. 8 (bead) and 9 (filament). The rate of diffusional mass transfer into the resin becomes less and less able to keep up with the rate of transport of solute through the column by the moving liquid as the flow rate increases.

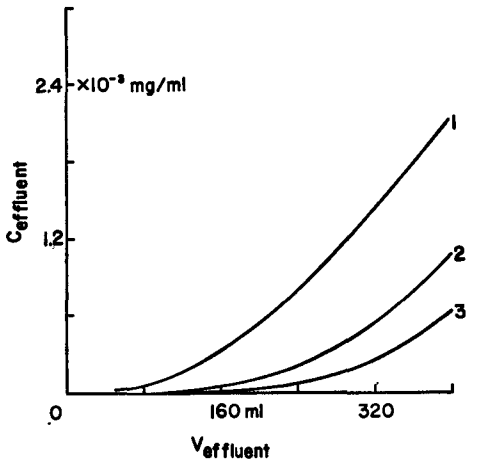

FIG. 4. Breakthrough curves for bead-packed columns. Effect of solute–resin diffusion constant. $r_b = 0.05$, $r_c = 1.0$, $l_c = 20$ cm; $Q = 1.0$ mL/sec; $c_{max} = 1.0$, $c^\circ = 10^{-2}$ mg/mL; $D = 2 \times 10^{-6}$ (1), 4×10^{-6} (2), 6×10^{-6} (3) cm²/sec; $V_r = 0.74$, $M = 30$, $K = 20$.

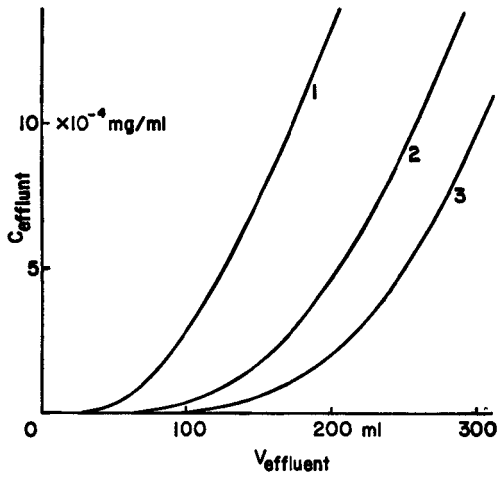

FIG. 5. Breakthrough curves for filament-packed columns. Effect of solute–resin diffusion constant. $r_f = 0.04$, $r_c = 1.0$, $l_c = 20$ cm; $Q = 1.0$ mL/sec; $c_{max} = 1.0$, $c^\circ = 10^{-2}$ mg/mL; $D = 2 \times 10^{-6}$ (1), 4×10^{-6} (2), 6×10^{-6} (3) cm²/sec; $V_r = 0.50$, $M = 30$, $K = 20$.

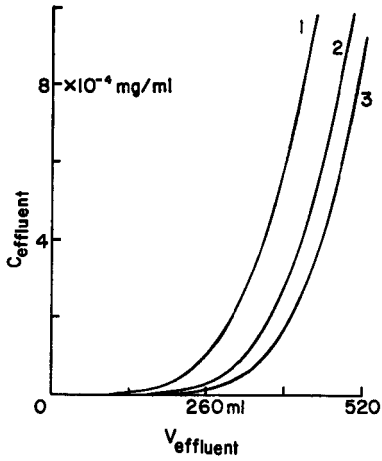

FIG. 6. Breakthrough curves for bead-packed columns. Effect of bead radius. $r_b = 0.05$ (1), 0.04 (2), 0.035 (3), $r_c = 1.0$, $l_c = 20$ cm; $Q = 1.0$ mL/sec; $c_{max} = 1.0$, $c^\circ = 10^{-2}$ mg/mL; $D = 6 \times 10^{-6}$ cm²/sec; $V_r = 0.74$, $M = 30$, $K = 20$.

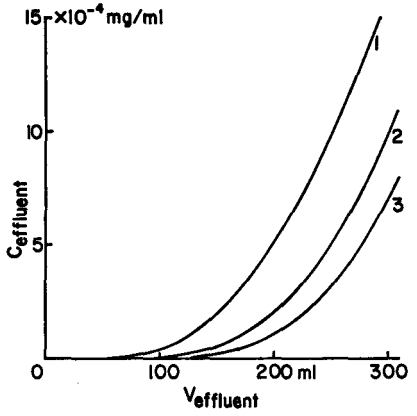

FIG. 7. Breakthrough curves for filament-packed columns. Effect of filament radius. $r_f = 0.05$ (1), 0.04 (2), 0.035 (3), $r_c = 1.0$, $l_c = 20$ cm; $Q = 1.0$ mL/sec; $c_{max} = 1.0$, $c^\circ = 10^{-2}$ mg/mL; $D = 6.0 \times 10^{-6}$ cm²/sec; $V_r = 0.50$, $M = 30$, $K = 20$.

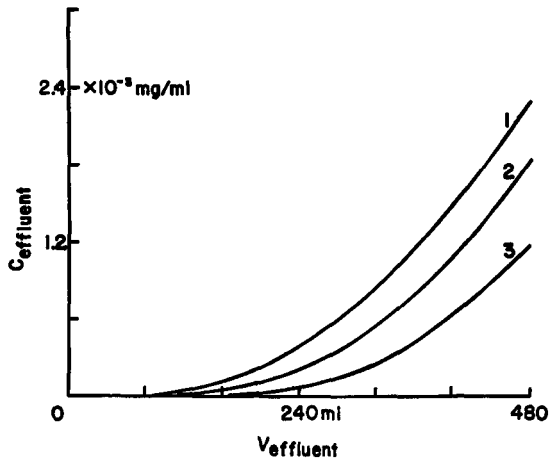

FIG. 8. Breakthrough curves for bead-packed columns. Effect of influent flow rate. $r_b = 0.05$, $r_c = 1.0$, $l_c = 20$ cm; $Q = 2.0$ (1), 1.5 (2), 1.0 (3) mL/sec; $c_{max} = 1.0$, $c^\circ = 10^{-2}$ mg/mL; $D = 6 \times 10^{-6}$ cm²/sec; $V_b = 0.74$, $M = 20$, $K = 20$.

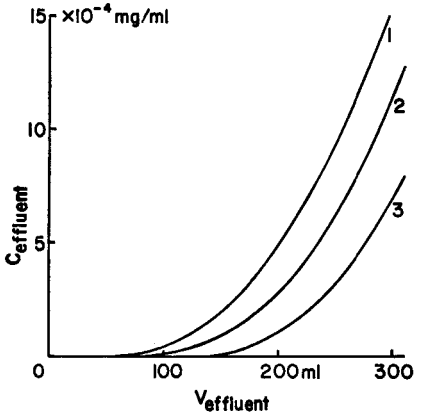

FIG. 9. Breakthrough curves for filament-packed columns. Effect of influent flow rate. $r_f = 0.035$, $r_c = 1.0$, $l_c = 20$ cm; $Q = 2.0$ (1), 1.5 (2), 1.0 (3) mL/sec; $c_{max} = 1.0$, $c^\circ = 10^{-2}$ mg/mL; $D = 6.0 \times 10^{-6}$ cm²/sec; $V_r = 0.50$, $M = 30$, $K = 20$.

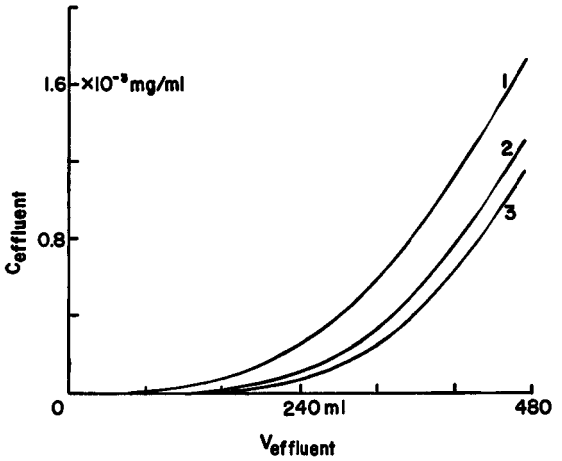

FIG. 10. Breakthrough curves for bead-packed columns. Effect of M, the number of slabs into which the column is partitioned (theoretical transfer units). $r_b = 0.05$, $r_c = 1.0$, $l_c = 20$ cm; $Q = 1.0$ mL/sec; $c_{max} = 1.0$, $c^\circ = 10^{-2}$ mg/mL; $D = 6 \times 10^{-6}$ cm²/sec; $V_r = 0.74$, $M = 10$ (1), 20 (2), 30 (3), $K = 20$.

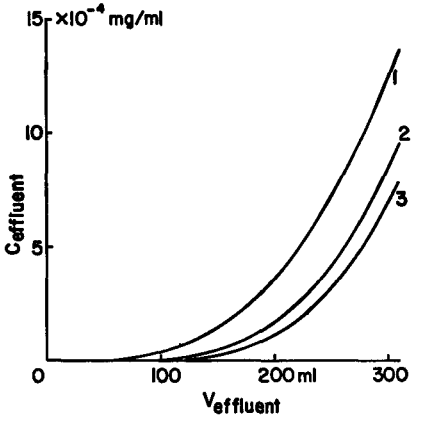

FIG. 11. Breakthrough curves for filament-packed columns. Effect of M, the number of slabs into which the column is partitioned (theoretical transfer units). $r_f = 0.035$, $r_c = 1.0$, $l_c = 20$ cm; $Q = 1.0$ mL/sec; $c_{max} = 1.0$, $c^\circ = 10^{-2}$ mg/mL; $D = 6 \times 10^{-6}$ cm²/sec; $V_r = 0.50$, $M = 10$ (1), 20 (2), 30 (3), $K = 20$.

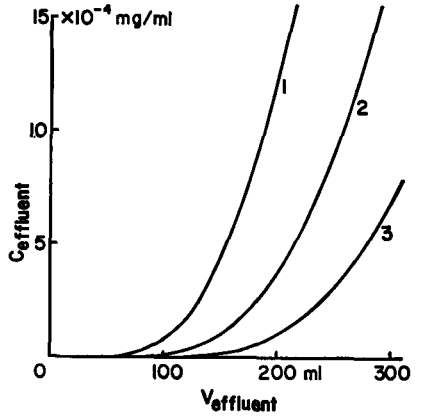

FIG. 12. Breakthrough curves for filament-packed columns. Effect of volume fraction resin. $r_f = 0.035$, $r_c = 1.0$, $l_c = 20$ cm; $Q = 1.0$ mL/sec; $c_{max} = 1.0$, $c^\circ = 10^{-2}$ mg/mL; $D = 6.0 \times 10^{-6}$ cm²/sec; $V_r = 0.30$ (1), 0.40 (2), 0.50 (3), $M = 30$, $K = 20$.

Figures 10 and 11 show the effect of varying the number of horizontal slabs into which the column is partitioned. The mathematical model assumes complete mixing of the liquid in each slab, so decreasing the number of slabs permits one to model an increase in axial dispersion of the liquid in the column. Axial dispersion can also be handled by including a finite difference approximation to a second derivative term in Eq. (32) or Eq. (65). This approach, however, uses more computer time than decreasing the number of slabs used to represent the column, and it leads to mathematical instability of the algorithm if the axial dispersion constant is large.

In columns packed with equal size spherical beads, the volume fraction resin is fixed in the vicinity of 0.74 unless the column is being operated in the fluidized bed mode. In filament-packed columns the volume fraction can in principle vary from 0 to 0.907. In Fig. 12 we see the effect of varying the volume fraction in filament-packed columns. The expected increase in effluent volume to breakthrough with increasing volume fraction resin is seen to occur.

We conclude that the behavior of macroreticular resin columns modeled in the way outlined here is certainly in agreement with one's qualitative expectations based on physical intuition, and we would anticipate little difficulty selecting model parameters to match experimental data. This approach is well adapted to modeling the effects of influents having time-dependent flow rates and compositions, so that the response of the system to pulse shock loadings can easily be studied. We note that columns packed with spheres absorb solute more rapidly than columns packed with the same volume of filaments of the same diameter—hardly surprising since the water–resin interfacial area of the sphere-packed column is 50% larger than that of the filament-packed column. However, if these resins could be prepared in thin filaments, one could obtain columns having short detention times which would not have the large hydraulic head losses bound to occur if spheres of similar diameter were used.

Acknowledgment

This work was supported by a grant from the Vanderbilt University Research Council.

REFERENCES

1. W. A. Aue, S. Kapila, and C. R. Hastings, *J. Chromatogr.*, *73*, 99 (1972).
2. W. Bertsch, E. Anderson, and G. Holzer, *Ibid.*, *112*, 701 (1975).
3. A. K. Burnham, G. V. Calder, J. S. Fritz, G. A. Junk, H. J. Svec, and R. Willis, *Anal. Chem.*, *44*, 139 (1972).

4. W. H. Glaze, J. E. Henderson IV, J. E. Bell, and V. A. Wheeler, *J. Chromatogr. Sci.*, *11*, 580 (1973).
5. G. A. Junk, J. J. Richard, M. D. Grieser, D. Witiak, J. L. Witiak, M. D. Arguello, R. Vic, H. J. Swec, J. S. Fritz, and G. V. Calder, *J. Chromatogr.*, *99*, 745 (1974).
6. W. H. Glaze, G. R. Peyton, and R. Rawley, *Environ. Sci. Technol.*, *11*, 685 (1977).
7. J. F. K. Huber and R. R. Becker, *J. Chromatogr.*, *142*, 765 (1977).
8. D. J. Pietrzyk and C.-H. Chu, *Anal. Chem.*, *49*, 757 (1977).
9. D. Paschal, R. Bicknell, and K. Siebenmann, *J. Environ. Sci. Health, B, 13*, 105 (1978).
10. M. Suzuki, Y. Yamato, and T. Akiyama, *Water Res.*, *12*, 777 (1978).
11. A. Tateda and J. S. Fritz, *J. Chromatogr.*, *152*, 329 (1978).
12. D. C. Kennedy, *Environ. Sci. Technol.*, *7*, 138 (1973).
13. L. A. Spano, R. A. Chalk, J. T. Walsh, and C. DiPietro, *Pollution Engineering and Science Solutions, Proceedings of an International Meeting of the Society for Engineering and Science, 1st*, 1973, p. 288; *Chem. Abstr.*, *78*, 163723n (1973).
14. B. R. Kim, V. L. Snoeyink, and F. M. Saunders, *J. Water Pollut. Control Fed.*, *48*, 120 (1976).
15. D. S. Farrier, A. L. Hines, and S. W. Wang, *J. Colloid Interface Sci.*, *69*, 233 (1979).
16. Rohm and Haas Co., *Summary Bulletin Amberlite Polymer Adsorbents*, Philadelphia, 1978, and technical notes or bulletins on Amberlite XAD-1, 2, 4, 7, and 8.
17. A. N. Clarke and D. J. Wilson, *Sep. Sci. Technol.*, *14*, 227 (1979).
18. D. J. Wilson, *Ibid.*, *14*, 415 (1979).
19. L. G. Kelly, *Handbook of Numerical Methods and Applications*, Addison-Wesley, Reading, Massachusetts, 1967, p. 186.
20. J. H. Clarke, A. N. Clarke, and D. J. Wilson, *Sep. Sci. Technol.*, *13*, 767 (1978).
21. A. N. Clarke, D. J. Wilson, and J. H. Clarke, *Ibid.*, *13*, 895 (1978).
22. D. J. Wilson, A. N. Clarke, and R. H. French, *Ibid.*, *14*, 1 (1979).
23. J. M. Brown, Ph.D. Dissertation, Vanderbilt University, Nashville, Tennessee, 1981.

Received by editor February 21, 1980